Cerebral Cortex, October 2020;30: 5229–5241

doi: 10.1093/cercor/bhaa085
Advance Access Publication Date: 29 May 2020
Original Article

ORIGINAL ARTICLE

Dynamic Reconfiguration, Fragmentation, and Integration of Whole-Brain Modular Structure across Depths of Unconsciousness

Dominic Standage[1], Corson N. Areshenkoff[2,3], Joseph Y. Nashed[2], R. Matthew Hutchison[4], Melina Hutchison[5], Dietmar Heinke[1], Ravi S. Menon[6], Stefan Everling[6,7] and Jason P. Gallivan[2,3,8]

[1]School of Psychology, University of Birmingham, B15 2TT, Birmingham, UK, [2]Centre for Neuroscience Studies, Queen's University, Kingston, K7L 3N6, Ontario, Canada, [3]Department of Psychology, Queen's University, Kingston, K7L 3N6, Ontario, Canada, [4]Biogen, Cambridge, 02142, MA, USA, [5]Massachusetts Eye and Ear Infirmary, Boston, 02114, MA, USA, [6]Robarts Research Institute, University of Western Ontario, London, N6G 2V4, Ontario, Canada, [7]Department of Physiology and Pharmacology, University of Western Ontario, N6A 5C1, London, Ontario, Canada and [8]Department of Biomedical and Molecular Sciences, Queen's University, K7L 3N6, Kingston, Ontario, Canada

Address correspondence to Dominic Standage, School of Psychology, University of Birmingham, Birmingham, UK. Email: d.standage@bham.ac.uk and Jason Gallivan, Centre for Neuroscience Studies, Queen's University, Kingston, Ontario, Canada. Email: gallivan@queensu.ca.

Abstract

General anesthetics are routinely used to induce unconsciousness, and much is known about their effects on receptor function and single neuron activity. Much less is known about how these local effects are manifest at the whole-brain level nor how they influence network dynamics, especially past the point of induced unconsciousness. Using resting-state functional magnetic resonance imaging (fMRI) with nonhuman primates, we investigated the dose-dependent effects of anesthesia on whole-brain temporal modular structure, following loss of consciousness. We found that higher isoflurane dose was associated with an increase in both the number and isolation of whole-brain modules, as well as an increase in the uncoordinated movement of brain regions between those modules. Conversely, we found that higher dose was associated with a decrease in the cohesive movement of brain regions between modules, as well as a decrease in the proportion of modules in which brain regions participated. Moreover, higher dose was associated with a decrease in the overall integrity of networks derived from the temporal modules, with the exception of a single, sensory-motor network. Together, these findings suggest that anesthesia-induced unconsciousness results from the hierarchical fragmentation of dynamic whole-brain network structure, leading to the discoordination of temporal interactions between cortical modules.

Key words: anesthesia, connectivity, consciousness, isoflurane, resting-state functional MRI, unconsciousnesswhole-brain dynamics

Introduction

Consciousness is the state of wakefulness and awareness characterized by the ability to receive and respond to sensory stimuli, and its biological basis has long fascinated neuroscientists, psychologists, and clinicians alike. This fascination not only stems from the broad implications of consciousness for understanding human conscious experience but also because disruptions in consciousness are a hallmark of both pathological (neurology)

and naturally occurring physiological states (sleep) and are often purposefully induced in clinical treatment (anesthesiology). In this regard, the neuroscientific investigation of consciousness has been greatly advanced in recent decades by the study of the unconscious state. Considerable work now focuses on changes in brain states that accompany normal and pathological conditions like sleep and coma, respectively (Mashour and Hudetz 2018). Likewise, the pharmacological induction and reversible manipulation of consciousness by general anesthesia has proven to be a highly productive line of investigation. While much of this latter work has focused on the cellular effects of anesthetics (Anis et al. 1983; Peduto et al. 1991; Wu et al. 1996), it remains poorly understood how these local effects manifest as unconsciousness at the large-scale, global level (Franks 2006; Alkire et al. 2008; Brown et al. 2011).

According to integrated information theory (Tononi 2004), consciousness is linked to the ability to integrate information both locally and between widely distributed brain areas. Information integration is also a fundamental principle of global neuronal workspace theory (Dehaene et al. 2014), which posits critical roles for long-distance interactions between brain regions in prefrontal, parietal, and cingulate cortex during general awareness. These theories suggest that general anesthetics impair functional interactions across remote brain areas, causing the fragmentation of whole-brain networks (Mashour and Hudetz 2018). Integrated information theory further posits that consciousness is not a fixed state per se but is graded in nature, decreasing proportionately with the number of discriminable brain states (Tononi et al. 2016). This gradient further suggests that interactions between brain networks (and consequently information integration) diminish beyond the initial threshold of unconsciousness (light sedation), with greater fragmentation occurring at deeper levels of sedation. Thus, investigation of the dose-dependent effects of anesthesia on whole-brain networks not only quantifies the effects of sedation on the global properties of neural processing but also serves to characterize the very nature of unconsciousness.

In recent years, resting-state functional MRI (rs-fMRI) has provided tremendous insight into the large-scale, network-level effects of anesthesia. rs-fMRI measures statistical dependencies between the slow-wave blood oxygenation level-dependent (BOLD) signal in distinct brain regions in the absence of any task paradigm (Biswal et al. 1995). These spontaneous, low-frequency fluctuations (0.01–0.1 Hz) of the BOLD signal have been shown to reflect underlying changes in neural activity, where correlations in the BOLD signal between areas (i.e., FC) correspond to known patterns of whole-brain connectivity in multiple species (Fox and Raichle 2007; Vincent et al. 2007; Shmuel and Leopold 2008; Hutchison and Everling 2012; Hutchison et al. 2012, 2015; Leopold and Maier 2012). Initially, the effects of anesthesia on FC were largely focused on activity within selected networks of areas and were assessed by constructing static functional networks from full scans (Vincent et al. 2007; Boveroux et al. 2010; Deshpande et al. 2010; Liu et al. 2011, 2013). Over these longer timescales (i.e., a full-length resting-state scan), functional networks may appear similar during levels of wakefulness and anesthesia (Barttfeld et al. 2015), since static measurements of FC may largely recapitulate the underlying anatomical map (Honey et al. 2009; Hermundstad et al. 2013). There is a growing appreciation, however, that functional networks are temporally dynamic (Chang and Glover 2010; Bassett et al. 2011; Hutchison, Womelsdorf, Allen, et al. 2013a; Hutchison, Womelsdorf, Gati, et al. 2013b; Allen et al. 2014) and that an understanding of whole-brain computation requires time-resolved methods for network analysis (Medaglia et al. 2015; Bassett and Sporns 2017).

In the study of unconsciousness, changes in the repertoire of whole-brain states derived from functional networks constructed over short timescales (e.g., 30 s—1.5 min) have been shown to correlate with anesthetic dose (Hutchison et al. 2014; Barttfeld et al. 2015; Hudetz et al. 2015; Uhrig et al. 2018). Specifically, it has been reported that the number of discriminable brain states decreases at deeper levels of unconsciousness, consistent with predictions by integrated information theory (Tononi et al. 2016). Together with static FC analyses demonstrating the fragmentation of networks during unconsciousness (Achard et al. 2012; Boly et al. 2012; Spoormaker et al. 2012; Monti et al. 2013; Hutchison et al. 2014), this finding implies that the temporal dynamics of network modularity may be highly informative. Modularity refers to the degree to which networks can be decomposed into groups of nodes (brain regions), with dense connectivity within these groups and sparse connectivity between them (formally quantifying fragmentation) (Sporns and Betzel 2016). Modular structure has long been recognized as a crucial property of complex biological systems, conferring functional specialization and robustness to change (including damage) (Kirschner and Gerhart 1998; Kashtan and Alon 2005; Wagner 2005). Analyses of task-based changes to modular structure have been highly productive in recent studies of the whole-brain bases of motor skill acquisition (Bassett et al. 2011, 2015) and cognitive performance (Braun et al. 2015), but to the best of our knowledge, no studies have leveraged these methods in the study of unconsciousness (see the Discussion for a summary of earlier studies using static measures of modularity).

We examined the dose-dependent effects of isoflurane on the temporal modular structure of whole-brain networks in nonhuman primates, following induction of unconsciousness. We tested three principal hypotheses. First, we sought to determine whether, under our time-resolved approach, there would be greater fragmentation of whole-brain networks at increased levels of isoflurane dose. Thus, we tested the hypothesis that the number of temporal modules, and their degree of modularity, will increase with isoflurane dose. Second, we reasoned that if the strength of connectivity within brain networks decreases with increasing dose (e.g. Boveroux et al. 2010; Guldenmund et al. 2013), then smaller perturbations (e.g., background noise) may be sufficient to drive small, random network reconfigurations, leading to uncoordinated changes in modular membership. We therefore quantified the degree to which brain regions move between modules in a coordinated (and uncoordinated) manner at different levels of dose. Third, we sought to determine the extent to which dynamic whole-brain structure would break down in a spatially uniform versus selective manner at deeper levels of unconsciousness. Thus, we derived networks from the temporal modules and tested the null hypothesis that the strength of interactions within and between those networks would decrease in a uniform fashion across networks with increasing isoflurane dose.

Materials and Methods

To examine the effects of general anesthesia on whole-brain temporal modular structure following the induction of unconsciousness, we collected rs-fMRI data from five nonhuman primates at increasing levels of isoflurane dose at 7-T MRI. To examine the incremental, dose-dependent effects of isoflurane

on temporal module dynamics, we administered isoflurane in six stepwise increments: 1.00%, 1.25%, 1.50%, 1.75%, 2.00%, and 2.75% (see Fig. 1A for an overview of our approach). We terminated the session for one monkey that experienced abnormal breathing patterns when the isoflurane concentration was increased to 2.75%, so no data were acquired from that monkey at that particular dose.

Following the parcellation of each animal's cerebrum into discrete brain regions, the time series correlation was computed between each pair of regions in sliding, half-overlapping windows, resulting in FC matrices for each window. We then constructed mutlislice networks from these FC matrices and partitioned them into temporal modules that maximized a quality function Q (Mucha et al. 2010) (see Fig. 1C). [The same measure was calculated for three established classes of null networks (Mucha et al. 2010; Bassett et al. 2011), verifying that subjects' whole-brain networks exhibited significant modularity (Supplementary Figure 2)]. We then characterized various features of modular reconfiguration across dose levels, as well as a summary measure of the modules themselves.

Animal Preparation

Five macaque monkeys (*Macaca fascicularis*; four females, weights ranging from 3.6 to 5.3 kg [mean ± standard deviation (SD) = 4.26 ± 0.76 kg] and ages ranging from 7.71 to 8.22 years [mean ± SD = 7.83 ± 0.22 years]), were involved in the experiment. All surgical and experimental procedures were carried out in accordance with the Canadian Council of Animal Care policy on the use of laboratory animals and approved by the Animal Use Subcommittee of the University of Western Ontario Council on Animal Care. Note that the use of an animal model for investigating the effects of anesthesia on brain activity offers greater standardization between subjects and circumvents concerns of potentially inducing a lethal collapse of the cardiovascular or respiratory system at high dosage in humans. The complete methods for this experiment have previously been described in detail (Hutchison et al. 2014). We therefore provide a more concise description of the methods relevant to our temporal analyses.

Prior to image acquisition, monkeys were injected intramuscularly with atropine (0.4 mg/kg), ipratropium (0.025 mg/kg), and ketamine hydrochloride (7.5 mg/kg), followed by intravenous administration of 3 mL propofol (10 mg/mL) via the saphenous vein. Animals were then intubated and switched to 1.5% isoflurane mixed with medical air. Each monkey was then placed in a custom-built monkey chair and inserted into the magnet bore, at which time the isoflurane level was lowered to 1.00%. Prior to image localization, shimming, and echo-planar imaging (EPI), at least 30 min was allowed for the isoflurane level and global hemodynamics to stabilize at this 1.00% concentration. [Given the rapid recovery properties of propofol (e.g. Flaishon et al. 1997), it is unlikely that any isoflurane-dependent effects are attributable to the initial propofol induction]. We then acquired two functional EPI scans at each of six increasing isoflurane levels: 1.00%, 1.25%, 1.50%, 1.75%, 2.00%, and 2.75% (0.78, 0.98, 1.17, 1.37, 1.56, and 2.15 minimum alveolar concentration [MAC], respectively). We interleaved a 10-min period between each increase in isoflurane dose to allow for the concentration to stabilize (during this 10-min period, we did not collect data). Throughout the duration of scanning, the monkeys spontaneously ventilated, and we monitored physiological parameters (temperature, oxygen saturation, heart rate, respiration, and end-tidal CO_2) to ensure that values were within normal limits (see Supplementary Figure 1 in Hutchison et al., 2014). The acquisitions of two anatomical images occurred during the stabilization periods between isoflurane dose levels.

Data Acquisition

The monkeys were scanned on an actively shielded 7-Tesla 68-cm horizontal bore scanner with a DirectDrive console (Agilent, Santa Clara, California) with a Siemens AC84 gradient subsystem (Erlangen, Germany). We used a custom in-house conformal five-channel transceive primate-head Radio Frequency (RF) coil. Each functional run consisted of 150 continuous EPI functional volumes (repetition time [TR] = 2000 ms; echo time [TE] = 16 ms; flip angle = 70^0; slices = 36; matrix = 96×96; Field of view [FOV] = 96×96 mm^2; acquisition voxel size = $1 \times 1 \times 1$ mm^3), acquired with GRAPPA = 2. A high-resolution gradient-echo T2 anatomical image was acquired along the same orientation as the functional images (TR = 1100 ms, TE = 8 ms, matrix = 256×256, FOV = 96×96 mm^2, acquisition voxel size = $375 \times 375 \times 1000$ mm^3). We also acquired a T1-weighted anatomical image (TE = 2.5 ms, TR = 2300 ms, FOV = 96×96 mm^2, acquisition voxel size = $750 \times 750 \times 750$ mm^3).

Image Preprocessing and Analysis

Functional image preprocessing was implemented in the FMRIB Software Library toolbox (FSL; http://www.fmrib.ox.ac.uk). This consisted of motion correction (six-parameter affine transformation), brain extraction, spatial smoothing (Gaussian kernel of full width at half maximum 3 mm applied to each volume separately), high-pass temporal filtering (Gaussian-weighted least squares straight line fitting with sigma = 100 s), and low-pass temporal filtering (half width at half maximum = 2.8 s, Gaussian filter). Functional data were nonlinearly registered to the T2 anatomical (FNIRT; http://www.fmrib.ox.ac.uk/fsl/fslwiki/FNIRT), then registered to the T1 anatomical (six degrees of freedom rigid transformation), and finally normalized (12 degrees of freedom linear affine transformation) to the F99 atlas template (Van Essen 2004) (see http://sumsdb.wustl.edu/sums/macaquemore.do).

The F99 template-normalized Lewis and van Essen (Lewis and Van Essen 2000a, 2000b) divisions were used to define 174 (87 per hemisphere) cortical regions (see Supplementary Figure 1 for an overview of these regions). Following regression of the average white matter (WM), cerebrospinal fluid (CSF), and six motion parameters from the regional time series, we calculated the mean time series for each region by averaging the time series across all voxels contained within it and then z-scored the time series within each scan (statistics of the non-z-scored time series are shown in Supplementary Figure 3). Note that we did not use regions from subcortical structures, due to concerns about anatomically based parcellation of small substructures and decreased signal-to-noise ratio.

There is mounting evidence that variation in FC between regions and networks that occurs during the resting state reflects real neural processes that are ignored in standard resting-state investigations that examine FC over the entire resting-state time window (Chang and Glover 2010; Hutchison, Womelsdorf, Allen, et al. 2013a; Hutchison, Womelsdorf, Gati, et al. 2013b; Allen et al. 2014). To explore the potential effects of isoflurane dose on time-varying network dynamics, each of the 174 regional time series was divided into windows of 60 s

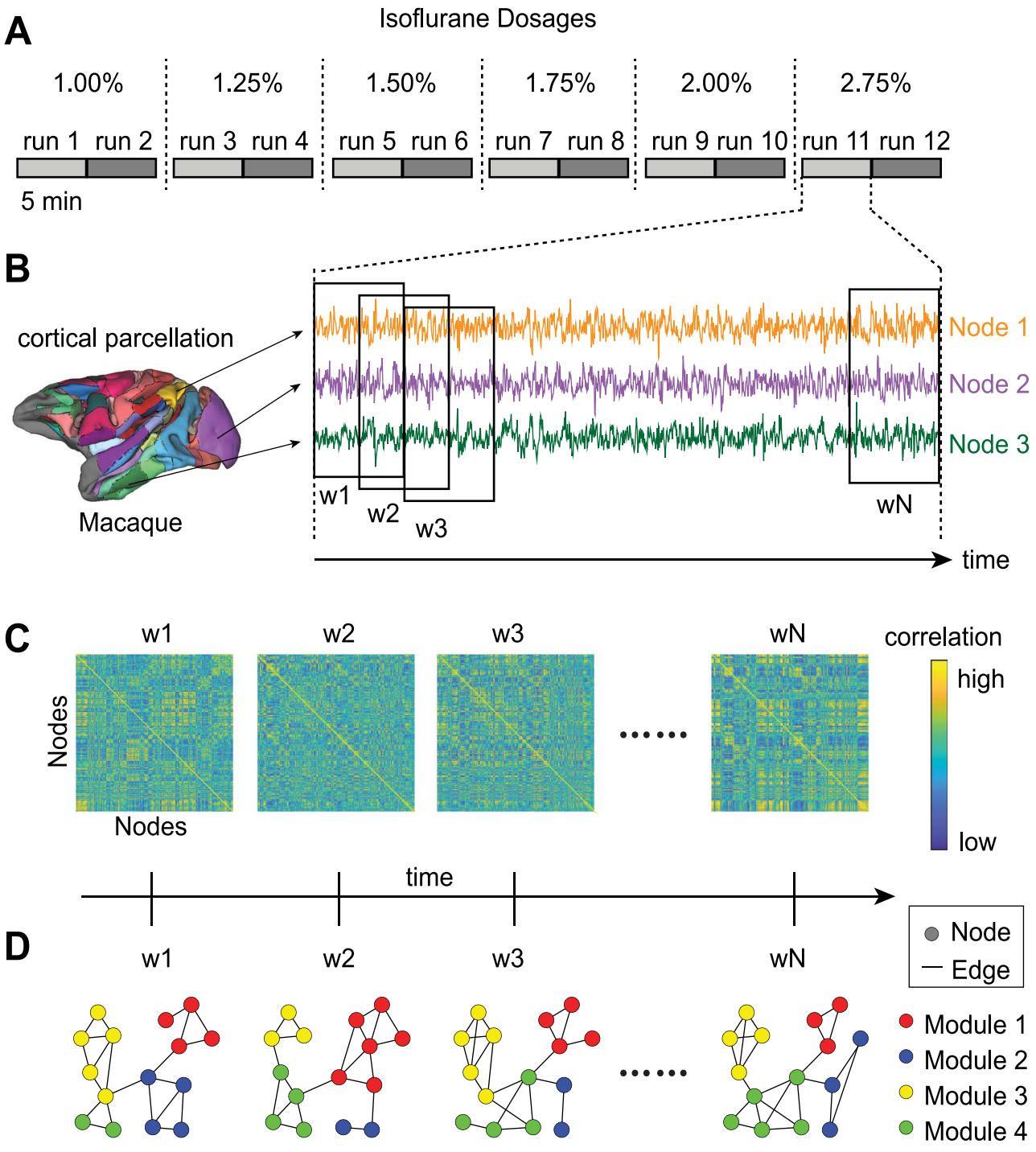

Figure 1. Overview of experiment and analysis approach. (*A*) For each animal, two 5-min resting-state scans were collected at each of the six isoflurane dose levels. (*B*) Each animal's cerebrum was parcellated into 174 discrete brain regions, and the average BOLD time series was extracted from each region (three example regions shown). (*C*) The Pearson correlation coefficient was calculated for each pair of regions in sliding, half-overlapping windows (shown in *B*), resulting in whole-brain functional connectivity (FC) matrices for each window (w1—wN). Together, these FC matrices can be used to construct a multislice (temporal) network for each subject and scan (see *D*). (*D*) Time-resolved clustering was then used to detect temporally dynamic modules in these networks (e.g., four modules in this schematic).

(30 imaging volumes) where contiguous windows overlapped by 50%. We constructed functional networks in each time window by calculating the Pearson correlation coefficient between each pair of brain regions (Fig. 1C). To mitigate against the possibility of spurious correlations ($P < 0.05$), all correlations that did not pass false discovery rate correction (Benjamini and Yekutieli 2001) were set to zero ($q = 0.05$), as were all negative correlations, a requirement of the module detection approach used (histograms and related statistics of positive and negative FC are shown in Supplementary Figure 4). We

determined the modular structure of the resulting multilayer (a.k.a. multislice) networks with a generalized Louvain method for time-resolved clustering (Jeub et al, http://netwiki.amath.unc.edu/GenLouvain, 2011–2017). This algorithm was repeated 100 times with random initialization, resulting in 100 clustering solutions (a.k.a. partitions). On each repetition, the algorithm was iterated until a stable partition was found, that is, the output on iteration n served as the input on iteration $n+1$ until the output matched the input (Mucha et al. 2010; Bassett et al. 2011). In this work, we used the standard spatial and temporal resolution parameters $\gamma = 1$ and $\omega = 1$, respectively (see the Supplementary Material for demonstrations of robustness). Note that our choice of window length served a balance between temporal resolution and mitigation against the effects of noise on network construction (Sakoğlu et al. 2010; Hutchison, Womelsdorf, Allen, et al. 2013a; Leonardi and Van De Ville 2015), while the overlap between windows served to increase the number of layers in the multilayer networks. Neither parameter was crucial to our results (see the Supplementary Material).

Statistical Analyses

Statistical analysis of these data is limited by the small number of subjects ($N = 5$) and the nonindependence of the data within each subject (Lazic 2010). Hierarchical modeling is an ideal solution to this problem, but models allowing for subject-specific effects are not easily fit to data sets as small as this one. We therefore used simple linear regression to model network statistics as a function of dose, which can be interpreted as assuming that all subjects respond identically to isoflurane. As shown in our Results, these models provided good fits overall, as intersubject variability was generally small relative to dose effects.

Results

Temporal Networks Become More Fragmented with Increasing Anesthetic Dose

To test the hypothesis that time-resolved modular structure becomes more fragmented with increasing levels of isoflurane dose, we calculated the mean number of modules over all partitions for each subject and scan (two scans per dose). The fit of a linear regression model to these data revealed a positive linear relationship between dose and number ($\beta_{dose} = 0.988$, $t(56) = 5.096$, $R^2 = 0.317$, $P = 4.236e-6$; see Fig. 2A). The SD of the number of modules across time windows showed a weak, negative linear relationship with dose ($\beta_{dose} = -0.05$, $t(56) = -2.129$, $R^2 = 0.075$, $P = 0.038$), suggesting that modular structure becomes more stable as it becomes more fragmented and explicitly demonstrating that the increased fragmentation does not reflect an increase in variability (Supplementary Figure 5). We also examined the relationship between dose and the quality function Q, capturing the degree to which whole-brain structure exhibits strong intramodule connectivity and sparse intermodule connectivity, i.e., higher Q corresponds to more isolated modules. A linear regression model revealed a similar relationship with dose as the number of modules ($\beta_{dose} = 0.039$, $R^2 = 0.231$, $t(56) = 4.107$, $P = 1.32e-4$; Fig. 2B). Together, these findings suggest that deeper levels of sedation partition the brain into a larger number of more isolated functional networks.

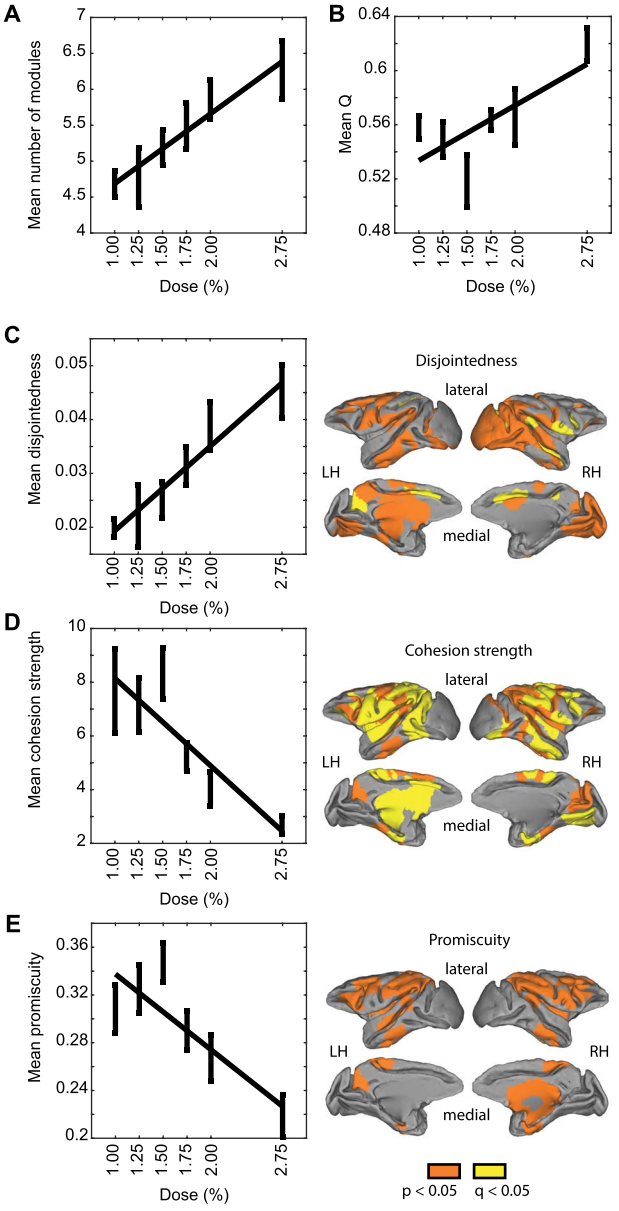

Figure 2. Isoflurane dose affects key properties of whole-brain temporal modules. (*A*) Mean number of temporal modules plotted as a function of isoflurane dose. In the plots, means were first taken over both scans for each dose and then taken over subjects. Error bars show ±1 standard error of the mean (SEM). Line shows the fit of a linear regression model to the across-subject means. (*B*) Mean Q, (*C*) mean disjointedness, (*D*) mean cohesion strength, and (*E*) mean promiscuity, calculated as in *A*. Right-side brain plots in panels *C*,–*E* show brain regions for which the relationship (Pearson correlation coefficient) between dose and the statistic on the left had a corresponding $P < 0.05$ (orange regions). Regions in yellow indicate those brain regions at $P < 0.05$ that further passed a false discovery rate correction (Benjamini and Hochberg 1995). The above linear fits were reproduced when both scans for each level of dose were concatenated (Supplementary Figure 6).

Whole-Brain Reconfiguration Becomes More Uncoordinated with Increasing Anesthetic Dose

To test our hypothesis that brain regions change modules in a more uncoordinated manner with increasing levels of isoflurane dose, we calculated the disjointed flexibility (disjointedness) of each brain region on each partition, defined as the

number of times the region changes modules independently (i.e., without other brain regions) relative to the total number of possible changes (Telesford et al. 2017). More formally, if N_{slice} is the number of time slices in a multislice network, $K(s)$ and $M(s+1)$ are the respective memberships of modules k and m at slices $s < N_{slice}$ and $s+1$, G is the set of regions moving from k to m at this time, and then region i moves disjointedly if and only if $i \in K(s)$, $i \in M(s+1)$ and $G = \{i\}$. Defining such disjointed movements by $d_i(s,s+1) = 1$ [0 otherwise], then disjointedness is defined for each region i by $D_i = \sum_{s,s+1} d_i/(N_{slice}-1)$. We calculated the mean disjointedness by taking the average over all regions on each partition, before taking the mean over these partition means (this procedure was also performed for all other region-specific measures; see below). The fit of a linear regression model revealed a positive linear relationship between dose and mean disjointedness ($\beta_{dose} = 0.016$, $t(56) = 5.422$, $R^2 = 0.344$, $P = 1.295e-6$; Fig. 2C). Based on this finding, we hypothesized that the opposite arrangement would also be true, that is, that brain regions would change modules in a more coordinated manner at lower levels of dose. To test this hypothesis, we calculated the strength of cohesive flexibility (cohesion strength) of each region on each partition, an independent measure from disjointedness (Telesford et al. 2017). We calculated this measure by first determining the number of times each region changes modules together with each other region and then summing over all other regions (Telesford et al. 2017). Following the above definitions, regions i and j move cohesively between modules k and m if and only if $\{i,j\} \subseteq K(s)$ and $\{i,j\} \subseteq M(s+1)$. Defining such cohesive movements by $cs_{i,j}(s,s+1) = 1$ [0 otherwise], then cohesion strength is defined for each region i by $CS_i = \sum_{s,s+1} \sum_{j \neq i} cs_{i,j}$. The fit of a linear regression model revealed a negative linear relationship between dose and mean cohesion strength ($\beta_{dose} = -3.276$, $t(56) = -5.648$, $R^2 = 0.363$, $P = 5.644e-7$; Fig. 2D). These complementary findings suggest that coordinated modular reconfiguration is a property of whole-brain dynamics under light sedation and that this property breaks down at deeper levels of sedation, such that smaller perturbations (e.g., noise) are sufficient to drive haphazard modular changes.

Modular Reconfiguration Becomes More Constrained with Increasing Anesthetic Dose

To further characterize modular changes as a function of dose, we calculated the promiscuity of each brain region, defined by the number of modules in which the region participates at least once, relative to the total number of modules (Sizemore and Bassett 2018). The fit of a linear regression model revealed a negative linear relationship between dose and promiscuity ($\beta_{dose} = -0.062$, $t(56) = -5.294$, $R^2 = 0.334$, $P = 2.068e-6$; Fig. 2E). This finding suggests that despite the fragmentation of whole-brain networks at deeper levels of sedation (Fig. 2A,B), brain regions do not participate in a broader repertoire of these modules.

Taken together, the above findings provide strong evidence that at deeper levels of sedation, 1) whole-brain networks become more fragmented and isolated, 2) individual brain regions move between modules in a more haphazard, uncoordinated manner, and 3) this haphazard movement between a larger number of modules does not entail more diverse modular participation by individual brain regions. Importantly, these results were highly robust across window sizes, the overlap between windows, and the resolution of time-resolved clustering (Supplementary Figure 7). Because the across-subject means in Figure 2B suggest that the relationship between dose and Q may be nonmonotonic (see Q values for dose levels of 1% and 1.5%), we fit a quadratic regression model to these data. The superior fit of the quadratic model was slightly nonmonotonic and compared favorably to the linear model according to information statistics (e.g., Akaike Information Criterion, corrected for small sample sizes). These results are shown in Supplementary Figure 8 and Supplementary Table 1. The respective fits of a quadratic model to dose and the number of modules, disjointedness, cohesion strength, and promiscuity were all monotonic (not shown).

Dynamic Network Architecture is Altered by Increasing Anesthetic Dose

To investigate whether isoflurane dose influences the degree to which groups of brain regions preferentially interact with one another, we determined the proportion of modular partitions (across all time windows of all scans for all subjects) in which each pair of brain regions was placed in the same module, referred to as a module allegiance matrix (Bassett et al. 2015). More specifically, we constructed a matrix T, where the elements $T_{i,j}$ refer to the number of times regions i and j were assigned to the same module over all time slices of all partitions for all subjects and scans. We then constructed the module allegiance matrix $MA = (1/C)T$, where C is the total number of time slices in all of these partitions. This matrix provides a summary of the brain network architecture associated with our isoflurane protocol. We then clustered the module allegiance matrix using symmetric nonnegative matrix factorization (see the Supplementary Methods and Supplementary Figure 9), identifying four clusters of regions corresponding to whole-brain networks. Because of the known degeneracy of the generalized Louvain algorithm [very different partitions can have nearly identical quality function scores (Bassett et al. 2011)], this clustering approach effectively identifies a consensus modularity partition (Bassett et al. 2013). In other words, it identifies a set of static brain networks summarizing the structure of the temporally dynamic modules from all partitions.

This summary network architecture and the module allegiance matrix from which it was derived are shown in Figure 3A,B. For comparison, Figure 3C shows the module allegiance matrix calculated for each level of isoflurane dose (across all time windows of both scans for all subjects, for each dose), labeled according to the four summary networks. Network 2, composed of regions in the visual, dorsal, parietal, and primary somatomotor cortex (yellow in Fig. 3B), appears to remain present across all six levels of dose (Fig. 3C), while the other networks (1, 3, and 4) appear to dissipate with increasing dose. Additionally, whereas the other networks appear to lose their distinctiveness from one another with increasing dose, Network 2 becomes increasingly isolated and even appears to fracture along hemispheric lines at the highest levels of dose (e.g., 2.00% and 2.75% isoflurane, see Fig. 3D).

Within- and Between-Network Integration Is Modulated by Anesthetic Dose

To quantify our observations of the module allegiance matrix, we estimated the integration of the four summary networks, within each network and between networks. With each brain region assigned to a network, the interaction between any

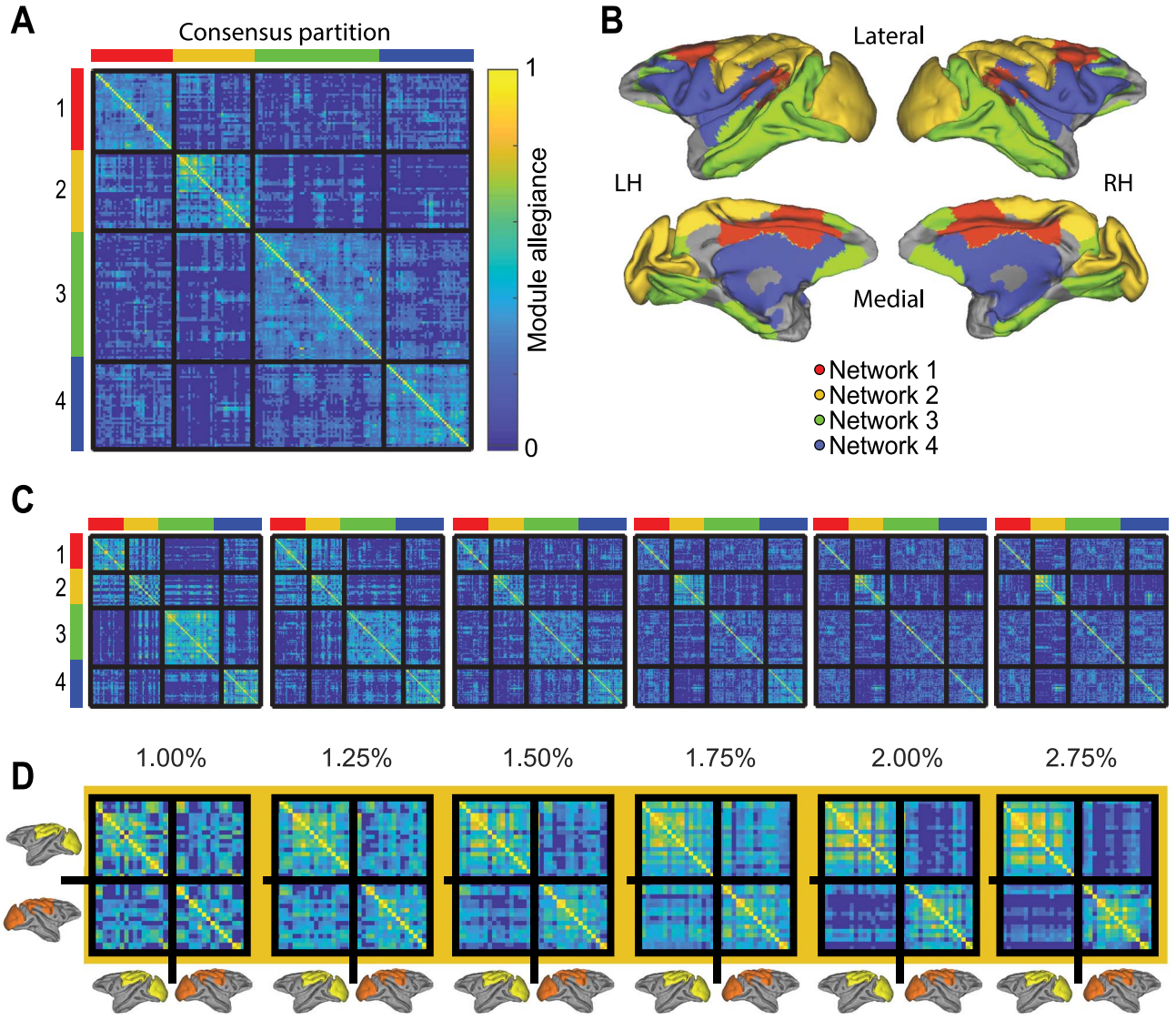

Figure 3. Summary architecture across levels of isoflurane dose. (*A*) Module allegiance matrix showing the probability of any two brain regions being part of the same temporal module across all subjects, scans and time windows. (*B*) Clustering of the module allegiance matrix in *A* identified a summary network architecture from the temporal modules, consisting of a cingulate–temporal–parietal–frontal network of regions (Network 1, red), a visual-somatomotor network (Network 2, yellow/orange), a temporal–parietal–prefrontal network (Network 3, green), and a lateral parietal–frontal cingulate temporal network (Network 4, blue). (*C*) The module allegiance matrix for each dose level, labeled according the summary network architecture in *A*. Note the relatively stable strength of allegiance in Network 2 across doses, compared to the decrease in allegiance in Networks 1, 3, and 4. (*D*) Magnified views of the visual-somatomotor network (Network 2) from *C*, which highlights a fracturing of this network along hemispheric lines at the highest dose levels (e.g., 2.00% and 2.75% isoflurane). The brain insets with yellow and orange regions denote the labelling of the module allegiance matrix with respect to the left and right hemispheric components of Network 2, respectively.

two networks can be measured by $I_{k1,k2} = (\sum i \in C_{k1}, j \in C_{k2} P_{i,j})/(|C_{k1}||C_{k2}|)$ (Bassett et al. 2015), where $C_{k\in1,2}$ are modules, $|C_k|$ is the number of regions they contain, and $P_{i,j}$ is the proportion of the time region i and j are in the same module. The interaction of a module with itself is calculated by allowing $k1 = k2$. The integration between two modules $k1 \neq k2$ is the normalized interaction between them $\prime_{k1,k2} = I_{k1,k2}/\sqrt{\left(I_{k1,k1} I_{k2,k2}\right)}$. We refer to the interaction of a network with itself as within-network integration and to the integration between different networks as between-network integration. [Note that "within-network integration" was referred to as "recruitment" in the task-based analysis from which we borrowed this method (Bassett et al. 2015).]

To quantify our observation that the majority of networks (all except the visual-somatomotor network) dissipated at higher levels of isoflurane dose, we fit a linear regression model to within-network integration as a function of dose for all subjects and scans. The model revealed a negative linear relationship between dose and within-network integration (Fig. 4A) for Network 1 ($\beta_{dose} = -2.368$, $t(56) = -6.3$, $R^2 = 0.415$, $P = 4.92e-8$), Network 3 ($\beta_{dose} = -4.238$, $t(56) = -6.078$, $R^2 = 0.397$, $P = 1.135e-7$), and Network 4 ($\beta_{dose} = -1.964$, $t(56) = -4.52$, $R^2 = 0.267$, $P = 3.252e-5$). Network 2, the visual-somatomotor network, did not show this relationship ($\beta_{dose} = -0.217$, $t(56) = -0.533$, $R^2 = -0.013$, $P = 0.596$). These findings confirm our observation that three of the four networks dissipated at deeper levels of sedation.

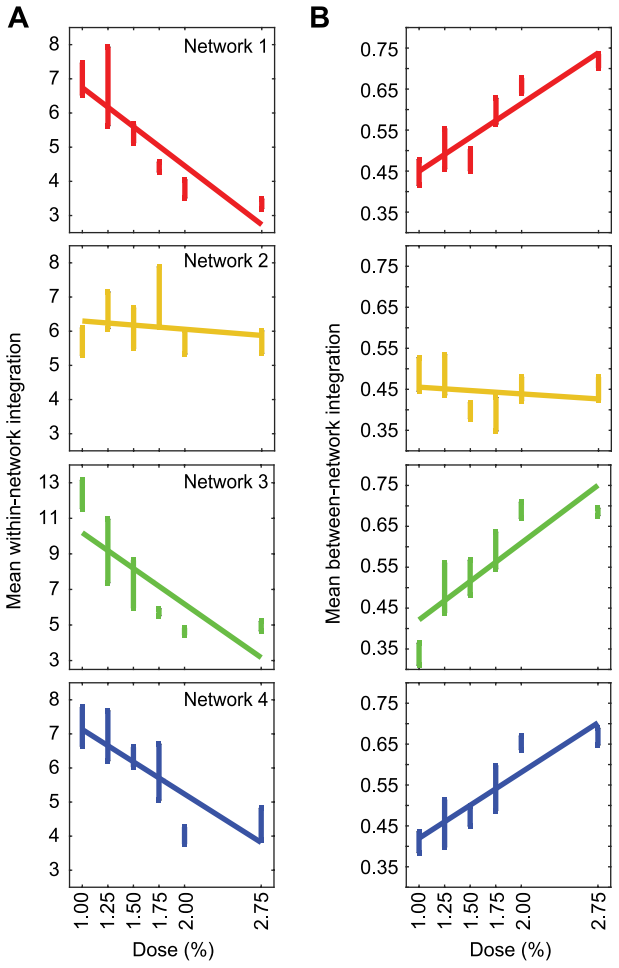

Figure 4. Within- and between-network integration is modified by isoflurane dose for all networks except for the visual-somatomotor network. (*A*) Within-network integration and (*B*) mean between-network integration of each network for each level of isoflurane dose. In the plots, means were taken over both scans for each dose and then over all subjects. Error bars show ±1 SEM. Lines show fits of a linear regression model to the across-subject means.

To quantify our observation that the majority of brain networks became less distinct with increasing isoflurane dose, we calculated the mean integration between each network and the other three networks. The fit of a linear regression model revealed a positive linear relationship between dose and mean between-network integration (Fig. 4B) for Network 1 ($\beta_{dose} = 0.168$, $t(56) = 7.559$, $R^2 = 0.505$, $P = 4.118e-10$), Network 3 ($\beta_{dose} = 0.196$, $t(56) = 7.151$, $R^2 = 0.477$, $P = 1.951e-9$), and Network 4 ($\beta_{dose} = 0.166$, $t(56) = 6.64$, $R^2 = 0.441$, $P = 1.357e-8$). Again, Network 2 was the exception, showing no such dose-dependent relationship with the other networks ($\beta_{dose} = -0.02$, $t(56) = -0.743$, $R^2 = 0.01$, $P = 0.46$). Furthermore, the integration between each pair of networks precisely tracked these mean interactions, that is, the integration between Networks 1, 3, and 4 showed a positive linear relationship with dose, whereas the integration between Network 2 (the visual-somatomotor network) and each of the other networks failed to show a dependence on dose (Supplementary Figure 10). Together, these findings confirm our observation that three out of four networks became less distinct with increasing isoflurane dose.

Network-Specific Effects on Region-Based Measures of Modular Reconfiguration

Lastly, having found network-specific differences for within-network and between-network integration, we sought to determine whether the movement of brain regions between temporal modules would also show differences according to network membership. We therefore calculated the mean disjointedness, cohesion strength, and promiscuity of each summary network, taking the same approach as above (Fig. 2C–E) but averaging these measures within each network, rather than across all brain regions. For each network, we fit a linear regression model to each measure of modular adaptability as a function of dose, finding that mean disjointedness increased with dose for all networks (Fig. 5A, left) and that mean cohesion strength (Fig. 5B, left) and promiscuity (Fig. 5C, left) decreased with dose for all networks. Across the 12 fits, R^2 values ranged from 0.173 to 0.384, and P values ranged from $0.01e-3$ to $2.13e-7$. Averaging across dose levels for each subject, the respective magnitudes of disjointedness (Fig. 5A, right) and promiscuity (Fig. 5C, right) were notably smaller in the visual-somatomotor network, while the magnitude of cohesion strength did not obviously differ between networks (Fig. 5B, right). Together, these findings suggest that the increase in uncoordinated modular reconfiguration at higher levels of sedation occurs globally throughout the brain but that the magnitude of the effect is smaller in primary sensory and motor areas (which make up the visual-somatomotor network).

Discussion

We investigated the dose-dependent effects of isoflurane on temporal modular structure in nonhuman primates following the induction of unconsciousness. Our analyses revealed that whole-brain structure became more fragmented at deeper levels of sedation, where the number and isolation of temporal modules increased with dose (Fig. 2A,B). When we characterized this modular reconfiguration at the level of brain regions, we found that deeper levels of sedation were associated with more uncoordinated movement of brain regions between modules, as revealed by an increase in disjointed flexibility (Fig. 2C) and a decrease in cohesive flexibility (Fig. 2D). Notably, this uncoordinated reconfiguration coincided with a proportional decrease in the number of modules in which brain regions participated, as measured by their promiscuity (Fig. 2E). Next, by determining the probability that each pair of brain regions was assigned to the same module over time, we identified four whole-brain networks that summarized subjects' dynamic whole-brain architecture across levels of sedation (Fig. 3A,B). Three out of four of these networks dissipated at deeper levels of sedation, as measured by their within-network (Fig. 4A) and between-network (Fig. 4B) integration. Interestingly, a lone network comprised of visual and somatomotor regions was impervious to these dose-dependent effects on integration. Together, our findings indicate that higher anesthetic dose results in the uncoordinated reconfiguration of modular structure across the cortex but that the breakdown in network structure is relatively spared in primary visual, somatosensory, and motor regions. These dose-dependent effects on whole-brain modular structure are consistent with the view that unconsciousness is graded in nature, selectively driven by disordered communication between circuits within the association cortex and other brain areas involved in integrative processes (Tononi et al.

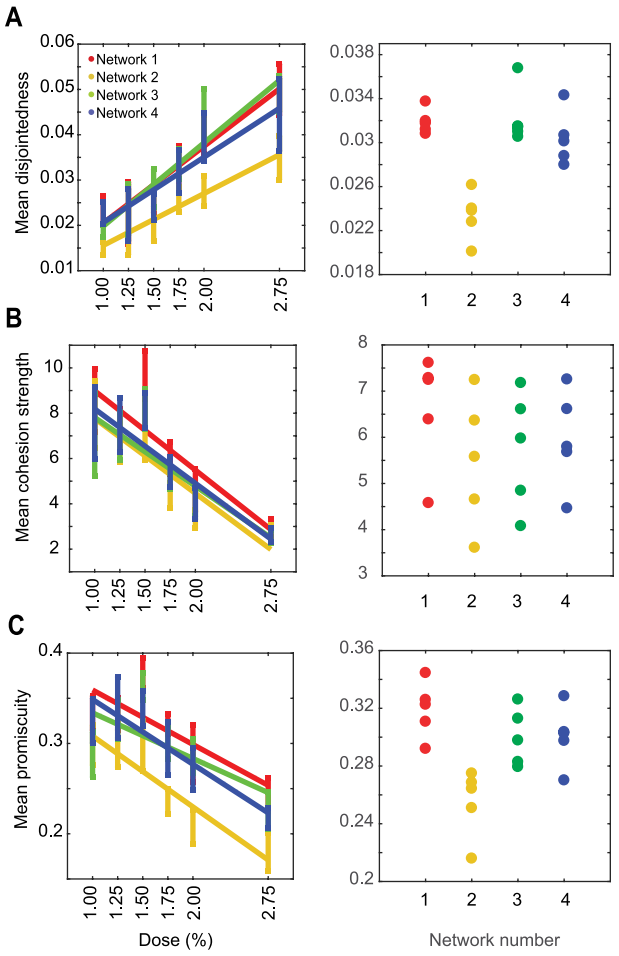

Figure 5. Mean disjointedness, cohesion strength, and promiscuity of each network. (*A*) Mean disjointedness for each level of isoflurane dose (left), where means were taken over both scans for each dose and then over all subjects. Error bars show ±1 SEM. Lines show fits from a linear regression model to the across-subject means. Distribution of subject means, taken over all doses, is shown on the right for each network. (*B*) Mean cohesion strength. (*C*) Mean promiscuity.

2016). As such, our results not only characterize changes in the dynamics of whole-brain network structure across depths of unconsciousness, but they characterize the global, network-level effects of different anesthetic doses in clinical treatment. Consequently, the neural measures of coordinated versus uncoordinated network reconfiguration reported here may offer potential diagnostic tools for identifying minimally conscious states or residual consciousness in vegetative state patients (Owen et al. 2006; Sitt et al. 2014).

Several earlier studies have used static module detection methods to characterize network fragmentation during unconsciousness (Achard et al. 2012; Boly et al. 2012; Spoormaker et al. 2012; Monti et al. 2013; Tagliazucchi et al. 2013; Hutchison et al. 2014), so it is important to differentiate the present methodology from those of these earlier investigations. Static module detection methods operate according to the same general principle as temporal module detection methods (i.e., they partition a network into modules that typically maximize the ratio of within-module to between module connectivity), but they do so for single-layer networks. Thus, even if these methods are used in each layer of a multilayer network constructed from windowed time series (e.g., Tagliazucchi et al. 2013), there is no formal relationship between a module in one time window and the modules in any other time window (Mucha et al. 2010; Bassett et al. 2011). Consequently, summary statistics (e.g., Q and the number of modules) can be computed over multiple time windows, but modular reconfiguration cannot be measured. Our temporal module analysis was in large part motivated by these earlier studies, which provided evidence for the increased fragmentation of whole-brain networks according to the number of static modules during isoflurane- (Monti et al. 2013; Hutchison et al. 2014) and propofol-induced (Monti et al. 2013) unconsciousness, as well as the magnitude of static modularity during propofol-induced unconsciousness (Monti et al. 2013) and sleep (Boly et al. 2012; Spoormaker et al. 2012; Tagliazucchi et al. 2013). Our finding that both Q (the magnitude of modularity, Fig. 2*B*) and the number of temporal modules (Fig. 2*A*) increased with dose offers novel support for the hypothesis that network fragmentation occurs in a graded fashion across levels of sedation. In this regard, it is important to note how these two measures are distinct. Q captures the degree to which modules are isolated from one another, but does not imply that more (or less) modules exist in a given partition. An increase in the number of modules with dose indicates a different kind of fragmentation altogether. Concurrently, these two findings further characterize a large body of evidence from static FC analyses that shows the breakdown of distributed networks, whereby brain networks decompose into a larger number of more isolated subnetworks during unconsciousness (MacDonald et al. 2015; Cavanna et al. 2018).

It is also important to note that maximal modularity does not equate to optimal modularity. While modules confer functional specialization and robustness, excessive modularity foregoes the advantages of integration over specialized subsystems (Kirschner and Gerhart 1998; Kashtan and Alon 2005; Wagner 2005). Thus, optimal modularity can be defined as a balance between these competing requirements. Our results imply that this balance is increasingly skewed toward specialization at deeper levels of unconsciousness, and we envision a continuum of optimal balance that peaks at higher levels of alertness during conscious processing. From this viewpoint, it is intuitive that connectivity between association cortical areas breaks down at lower levels of sedation than connectivity between sensory and motor systems. Integration over specialized subsystems is widely believed to be the role of the association cortex in the cortical hierarchy (Jones and Powell 1970; Kaas 1989), supporting the analytic and creative processing associated with awareness and higher cognitive function. Here, it is worth noting the intriguing similarity between the notion of optimal modularity and the foundational principles of integrated information theory, which posit that consciousness emerges from a balance between differentiation and integration of distributed computational components (Tononi et al. 2016). This balance is hypothesized to maximize systemic complexity, resulting in a large number of more diverse brain states, required to account for a large, diverse set of conscious experiences (Cavanna et al. 2018). Our finding that fragmentation (corresponding to differentiation) increased with dose appears to support this hypothesis. Future work should systematically explore the relationship between measurements of modularity and complexity in whole-brain networks and the dependence of this relationship on anesthetic dose.

The dose-dependent decrease in within-network integration in three out of four summary networks derived from temporal modules (Fig. 4*A*) accords with earlier evidence for the

breakdown of static networks at deeper levels of sedation (MacDonald et al. 2015), while the imperviousness of the visual-somatomotor network to this effect provides further evidence that the breakdown of network structure under suprathreshold anesthetic dose is spatially nonuniform, with primary sensory and motor cortical areas less affected than higher-order association cortical areas (He et al. 2008; Boveroux et al. 2010; Martuzzi et al. 2010; Liu et al. 2013; Hudetz et al. 2016). This general pattern of observations supports the view that unconsciousness results not from a breakdown in sensory processing per se but rather from a breakdown in integrative processing by higher-order brain networks involved in integrating and interpreting that sensory information (Hudetz 2006; Alkire et al. 2008).

At first glance, our finding that between-network integration across the majority of networks increased with dose (Fig. 4B) appears to conflict with earlier evidence showing a "decrease" in the integration between networks under anesthesia (MacDonald et al. 2015). However, we measured network integration relative to a module allegiance matrix, which describes the probability that regional pairs were assigned to the same module over time (Fig. 3A), not the magnitude of coactivation of their constituent regions (as is typical in static FC investigations). To reconcile these observations, we calculated the mean FC of our summary networks and found that it decreased with dose, both within and between networks (Supplementary Figure 11). Thus, the increase in between-network integration among three of four summary networks reflects a general weakening of network structure at higher levels of dose, rather than an increase in functional interactions. A thorough characterization of the dose dependence of FC is provided by Supplementary Figure 4. In addition, the preservation of the integrity of the visual-somatomotor network across levels of dose may reflect the overall reduction in FC, which tends toward the underlying structural connectivity (MacDonald et al. 2015). Our finding that the variability in the number of modules decreased with increasing dose (Supplementary Figure 5) is consistent with this possibility, which may account for earlier evidence that functional brain states become more stable at higher anesthetic dose (Hutchison et al. 2014; Barttfeld et al. 2015).

Our finding that disjointed flexibility increased with isoflurane dose (Fig. 2B) supports our hypothesis that weaker network structure should lead to more haphazard, uncoordinated changes in the affiliation of brain regions with modules. Likewise, our finding that cohesion strength decreased with increased isoflurane dose (Fig. 2C) is consistent with the decrease in whole-brain state transitions at higher dose (Hutchison et al. 2014; Barttfeld et al. 2015), assuming that such state transitions are more readily driven by groups of brain regions acting in concert than by individual brain regions. The inverse relationship between disjointedness and cohesion strength, which serve as two independent measures of regional flexibility (Telesford et al. 2017), suggests that these measures may also provide a useful marker for tracking levels of conscious processing. Prior work using dynamic connectivity methods has shown that the awake state is characterized by a rich and flexible repertoire of whole-brain states (Barttfeld et al. 2015; Uhrig et al. 2018) and that these states are expressed more frequently at lighter (compared to deeper) levels of sedation (Hutchison et al. 2014; Barttfeld et al. 2015). From this perspective, coordinated changes in modular structure may provide a neural signature of an engaged mind, suggesting that cohesive flexibility should correlate with the performance of demanding cognitive tasks, from learning (Telesford et al. 2017) and problem solving to creative thinking. Our finding that promiscuity was greater at lower isoflurane dose is consistent with this possibility, assuming that the exploration of a larger number of diverse brain states entails a broader range of modular reconfigurations and, correspondingly, a proportionally larger repertoire of modules in which brain regions participate. Future work should address these possibilities. Finally, it is worth noting that earlier work has shown correlations between modular flexibility in general (the relative frequency of changes in modular affiliation) and the performance of cognitive tasks (Braun et al. 2015) and it would be informative to subcharacterize flexibility as disjointed or cohesive in these data.

Our findings should be interpreted in light of several methodological considerations. Firstly, our study did not measure subjects' FC during the awake state, restricting our discussion to changes in network architecture during unconsciousness and at deepening levels of sedation. Secondly, because our study was focused on anesthetic-related changes in cortical brain networks, our current findings do not address the role of the thalamus, a site of suppression for many anesthetic agents (Alkire et al. 2000), in contributing to these cortical changes. Thirdly, because we used isoflurane in our study, we are unable to distinguish the extent to which our results reflect whole-brain properties of general anesthesia or the specific mechanisms of action of isoflurane. Fourthly, isoflurane has effects on cerebral blood flow and volume (Masamoto and Kanno 2012), leading to concerns that its neurovascular effects could obscure potential neural changes. We believe this effect is unlikely to explain our results, as studies using fMRI with electrophysiological recordings have indicated a close coupling between neural activity and hemodynamics under anesthesia (Vincent et al. 2007; Liu et al. 2013). Finally, we also recognize the inherent limits of fMRI in characterizing the dose-dependent effects of anesthesia, not only because of the limits of its spatial and temporal resolution but also because it provides an indirect assay (via hemodynamics) of underlying neural changes. We address these, and other considerations, in the Supplementary Material. Overall, we believe it is unlikely that our findings reflect the specific mechanisms of isoflurane or purely neurovascular effects, rather than neural effects.

Unconsciousness has been extensively characterized as a decrease in the integration of regional activity in whole-brain networks, both theoretically (Dehaene et al. 2014; Tononi et al. 2016) and experimentally (MacDonald et al. 2015; Cavanna et al. 2018). Two general mechanisms have been suggested to underlie this decrease (Hudetz 2006; Alkire et al. 2008). On the one hand, FC breaks down nonuniformly at suprathreshold levels of anesthesia, suggesting an overall decrease in correlated activity between brain regions (Peltier et al. 2005; Lu et al. 2007; Deshpande et al. 2010). On the other hand, a global decrease in functional segregation suggests a decrease in the specificity of connectivity (Liu et al. 2011, 2013; Kalthoff et al. 2013). Our results take an important step toward reconciling these observations, offering evidence in support of both views within a common framework. With respect to the first view, our finding that the integrity of three out of four summary networks diminished at deeper levels of sedation provides compelling evidence for the spatially nonuniform breakdown of network structure. With respect to the second view, our finding that both the strength of modularity and the number of modules increased at deeper levels of sedation implies an increase in functional segregation, rather than a decrease; however, our finding that the strength of FC decreased both within and between networks at

deeper levels of sedation (Supplementary Figure 11) is consistent with a general breakdown of network connectivity. Moreover, the dose-dependent increase in disjointedness, decrease in cohesion strength, and decrease in promiscuity occurred in all networks (Fig. 5A), further demonstrating global network-level effects. Indeed, we hypothesized that the global weakening of FC would render small background perturbations sufficient to drive uncoordinated modular changes (Fig. 2B). This weakening of FC and its effects on modular reconfiguration may underlie the dissipation of three out of four summary networks, since our module allegiance matrix quantified the probability that brain regions were grouped together in dynamic modules. Thus, in so far as our temporal modular approach addresses each of the core aspects of the two views, our findings suggest that they account for quantifiable expressions of the same underlying mechanism.

Supplementary Material

Supplementary material can be found at *Cerebral Cortex* online.

Funding

Canadian Institutes of Health Research (CIHR) (MOP126158 to J.P.G., MOP89785 to S.E., and PRG-165679 to R.M.); This research has been funded by the European Union's Horizon 2020 Research and Innovation Programme under the Marie Sklodowska-Curie grant agreement No 798255. Natural Sciences and Engineering Research Council (NSERC) graduate award (to C.N.A.). NSERC Discovery Grant, as well as funding from the Canadian Foundation for Innovation (to J.P.G.).

Notes

We thank Peter Mucha for the helpful advice on the generalized Louvain algorithm and Sarah Hughes for technical assistance.

Conflict of Interest

None declared.

References

Achard S, Delon-Martin C, Vértes PE, Renard F, Schenck M, Schneider F, Heinrich C, Kremer S, Bullmore ET. 2012. Hubs of brain functional networks are radically reorganized in comatose patients. *Proc Natl Acad Sci USA*. 109:20608–20613.

Alkire MT, Haier RJ, Fallon JH. 2000. Toward a unified theory of narcosis: brain imaging evidence for a thalamocortical switch as the neurophysiologic basis of anesthetic-induced unconsciousness. *Conscious Cogn*. 9:370–386.

Alkire MT, Hudetz AG, Tononi G. 2008. Consciousness and anesthesia. *Science*. 322:876–880.

Allen EA, Damaraju E, Plis SM, Erhardt EB, Eichele T, Calhoun VD. 2014. Tracking whole-brain connectivity dynamics in the resting state. *Cereb Cortex*. 24:663–676.

Anis NA, Berry SC, Burton NR, Lodge D. 1983. The dissociative anaesthetics, ketamine and phencyclidine, selectively reduce excitation of central mammalian neurones by N-methyl-aspartate. *Br J Pharmacol*. 79:565–575.

Barttfeld P, Uhrig L, Sitt JD, Sigman M, Jarraya B, Dehaene S. 2015. Signature of consciousness in the dynamics of resting-state brain activity. *Proc Natl Acad Sci USA*. 112:887–892.

Bassett DS, Porter MA, Wymbs NF, Grafton ST, Carlson JM, Mucha PJ. 2013. Robust detection of dynamic community structure in networks. *Chaos*. 23:013142.

Bassett DS, Sporns O. 2017. Network neuroscience. *Nat Neurosci*. 20:353–364.

Bassett DS, Wymbs NF, Porter MA, Mucha PJ, Carlson JM, Grafton ST. 2011. Dynamic reconfiguration of human brain networks during learning. *Proc Natl Acad Sci USA*. 108:7641–7646.

Bassett DS, Yang M, Wymbs NF, Grafton ST. 2015. Learning-induced autonomy of sensorimotor systems. *Nat Neurosci*. 18:744–751.

Benjamini Y, Hochberg Y. 1995. Controlling the false discovery rate: a practical and powerful approach to multiple testing. *J R Stat Soc B Methodol*. 57:289–300.

Benjamini Y, Yekutieli D. 2001. The control of the false discovery rate in multiple testing under dependency. *Ann Stat*. 29:1165–1188.

Biswal B, Yetkin FZ, Haughton VM, Hyde JS. 1995. Functional connectivity in the motor cortex of resting human brain using echo-planar MRI. *Magn Reson Med*. 34:537–541.

Boly M, Perlbarg V, Marrelec G, Schabus M, Laureys S, Doyon J, Pélégrini-Issac M, Maquet P, Benali H. 2012. Hierarchical clustering of brain activity during human nonrapid eye movement sleep. *Proc Natl Acad Sci USA*. 109:5856–5861.

Boveroux P, Vanhaudenhuyse A, Bruno M-A, Noirhomme Q, Lauwick S, Luxen A, Degueldre C, Plenevaux A, Schnakers C, Phillips C, et al. 2010. Breakdown of within- and between-network resting state functional magnetic resonance imaging connectivity during propofol-induced loss of consciousness. *Anesthesiology*. 113:1038–1053.

Braun U, Schäfer A, Walter H, Erk S, Romanczuk-Seiferth N, Haddad L, Schweiger JI, Grimm O, Heinz A, Tost H, et al. 2015. Dynamic reconfiguration of frontal brain networks during executive cognition in humans. *Proc Natl Acad Sci USA*. 112:11678–11683.

Brown EN, Purdon PL, Van Dort CJ. 2011. General anesthesia and altered states of arousal: a systems neuroscience analysis. *Annu Rev Neurosci*. 34:601–628.

Cavanna F, Vilas MG, Palmucci M, Tagliazucchi E. 2018. Dynamic functional connectivity and brain metastability during altered states of consciousness. *Neuroimage*. 180: 383–395.

Chang C, Glover GH. 2010. Time-frequency dynamics of resting-state brain connectivity measured with fMRI. *Neuroimage*. 50:81–98.

Dehaene S, Charles L, King J-R, Marti S. 2014. Toward a computational theory of conscious processing. *Curr Opin Neurobiol*. 25:76–84.

Deshpande G, Kerssens C, Sebel PS, Hu X. 2010. Altered local coherence in the default mode network due to sevoflurane anesthesia. *Brain Res*. 1318:110–121.

Flaishon R, Windsor A, Sigl J, Sebel PS. 1997. Recovery of Consciousness after Thiopental or Propofol. Bispectral Index and Isolated Forearm Technique. *Anesthesiology*. 86:613–19.

Fox MD, Raichle ME. 2007. Spontaneous fluctuations in brain activity observed with functional magnetic resonance imaging. *Nat Rev Neurosci*. 8:700–711.

Franks NP. 2006. Molecular targets underlying general anaesthesia. *Br J Pharmacol*. 147(Suppl 1):S72–S81.

Guldenmund P, Demertzi A, Boveroux P, Boly M, Vanhaudenhuyse A, Bruno M-A, Gosseries O, Noirhomme Q, Brichant J-F, Bonhomme V, et al. 2013. Thalamus, brainstem and salience network connectivity changes during

propofol-induced sedation and unconsciousness. *Brain Connect*. 3:273–285.

Sakoğlu Unal, Godfrey D. Pearlson, Kent A. Kiehl, Wang Y. Michelle, Andrew M. Michael, Vince D. Calhoun. 2010. A Method for Evaluating Dynamic Functional Network Connectivity and Task-Modulation: Application to Schizophrenia. 23:351–66.

He BJ, Snyder AZ, Zempel JM, Smyth MD, Raichle ME. 2008. Electrophysiological correlates of the brain's intrinsic large-scale functional architecture. *Proc Natl Acad Sci USA*. 105:16039–16044.

Hermundstad AM, Bassett DS, Brown KS, Aminoff EM, Clewett D, Freeman S, Frithsen A, Johnson A, Tipper CM, Miller MB, et al. 2013. Structural foundations of resting-state and task-based functional connectivity in the human brain. *Proc Natl Acad Sci USA*. 110:6169–6174.

Honey CJ, Sporns O, Cammoun L, Gigandet X, Thiran JP, Meuli R, Hagmann P. 2009. Predicting human resting-state functional connectivity from structural connectivity. *Proc Natl Acad Sci USA*. 106:2035–2040.

Hudetz AG. 2006. *Suppressing consciousness: Mechanisms of general anesthesia*. *Semin Anesth Perioperat Med Pain*.

Hudetz AG, Liu X, Pillay S. 2015. Dynamic repertoire of intrinsic brain states is reduced in propofol-induced unconsciousness. *Brain Connect*. 5:10–22.

Hudetz AG, Vizuete JA, Pillay S, Mashour GA. 2016. Repertoire of mesoscopic cortical activity is not reduced during anesthesia. *Neuroscience*. 339:402–417.

Hutchison RM, Everling S. 2012. Monkey in the middle: why non-human primates are needed to bridge the gap in resting-state investigations. *Front Neuroanat*. 6:29.

Hutchison RM, Gallivan JP, Culham JC, Gati JS, Menon RS, Everling S. 2012. Functional connectivity of the frontal eye fields in humans and macaque monkeys investigated with resting-state fMRI. *J Neurophysiol*. 107:2463–2474.

Hutchison RM, Matthew Hutchison R, Culham JC, Randall Flanagan J, Everling S, Gallivan JP. 2015. Functional subdivisions of medial parieto-occipital cortex in humans and nonhuman primates using resting-state fMRI. *Neuroimage*. 116:10–29.

Hutchison RM, Matthew Hutchison R, Hutchison M, Manning KY, Menon RS, Everling S. 2014. Isoflurane induces dose-dependent alterations in the cortical connectivity profiles and dynamic properties of the brain's functional architecture. *Hum Brain Mapp*. 35:5754–5775.

Hutchison RM, Womelsdorf T, Allen EA, Bandettini PA, Calhoun VD, Corbetta M, Della Penna S, Duyn JH, Glover GH, Gonzalez-Castillo J, et al. 2013a. Dynamic functional connectivity: promise, issues, and interpretations. *Neuroimage*. 80:360–378.

Hutchison RM, Womelsdorf T, Gati JS, Everling S, Menon RS. 2013b. Resting-state networks show dynamic functional connectivity in awake humans and anesthetized macaques. *Hum Brain Mapp*. 34:2154–2177.

Jones EG, Powell TP. 1970. An anatomical study of converging sensory pathways within the cerebral cortex of the monkey. *Brain*. 93:793–820.

Kaas JH. 1989. The evolution of complex sensory systems in mammals. *J Exp Biol*. 146:165–176.

Kalthoff D, Po C, Wiedermann D, Hoehn M. 2013. Reliability and spatial specificity of rat brain sensorimotor functional connectivity networks are superior under sedation compared with general anesthesia. *NMR Biomed*. 26:638–650.

Kashtan N, Alon U. 2005. Spontaneous evolution of modularity and network motifs. *Proc Natl Acad Sci USA*. 102:13773–13778.

Kirschner M, Gerhart J. 1998. Evolvability. *Proc Natl Acad Sci USA*. 95:8420–8427.

Lazic SE. 2010. The problem of pseudoreplication in neuroscientific studies: is it affecting your analysis? *BMC Neurosci*. 11:1–17.

Leopold DA, Maier A. 2012. Ongoing physiological processes in the cerebral cortex. *Neuroimage*. 62:2190–2200.

Leonardi Nora, Dimitri Van De Ville. 2015. On Spurious and Real Fluctuations of Dynamic Functional Connectivity during Rest. *NeuroImage*. 104:430–36.

Lewis JW, Van Essen DC. 2000a. Corticocortical connections of visual, sensorimotor, and multimodal processing areas in the parietal lobe of the macaque monkey. *J Comp Neurol*. 428:112–137.

Lewis JW, Van Essen DC. 2000b. Mapping of architectonic subdivisions in the macaque monkey, with emphasis on parieto-occipital cortex. *J Comp Neurol*. 428:79–111.

Liu X, Zhu XH, Zhang Y, Chen W. 2011. Neural origin of spontaneous hemodynamic fluctuations in rats under burst-suppression anesthesia condition. *Cereb Cortex*. 21:374–84.

Liu X, Zhu X-H, Zhang Y, Chen W. 2013. The change of functional connectivity specificity in rats under various anesthesia levels and its neural origin. *Brain Topogr*. 26:363–77.

Lu H, Zuo Y, Gu H, Waltz JA, Zhan W, Scholl CA, Rea W, Yang Y, Stein EA. 2007. Synchronized delta oscillations correlate with the resting-state functional MRI signal. *Proc Natl Acad Sci USA*. 104:18265–18269.

MacDonald AA, Naci L, MacDonald PA, Owen AM. 2015. Anesthesia and neuroimaging: investigating the neural correlates of unconsciousness. *Trends Cogn Sci*. 19:100–107.

Martuzzi R, Ramani R, Qiu M, Rajeevan N, Constable RT. 2010. Functional connectivity and alterations in baseline brain state in humans. *Neuroimage*. 49:823–834.

Masamoto K, Kanno I. 2012. Anesthesia and the quantitative evaluation of neurovascular coupling. *J Cereb Blood Flow Metab*. 32:1233–1247.

Mashour GA, Hudetz AG. 2018. Neural correlates of unconsciousness in large-scale brain networks. *Trends Neurosci*. 41:150–160.

Medaglia JD, Lynall M-E, Bassett DS. 2015. Cognitive network neuroscience. *J Cogn Neurosci*. 27:1471–1491.

Monti MM, Lutkenhoff ES, Rubinov M, Boveroux P, Vanhaudenhuyse A, Gosseries O, Bruno M-A, Noirhomme Q, Boly M, Laureys S. 2013. Dynamic change of global and local information processing in propofol-induced loss and recovery of consciousness. *PLoS Comput Biol*. 9:e1003271.

Mucha PJ, Richardson T, Macon K, Porter MA, Onnela J-P. 2010. Community structure in time-dependent, multiscale, and multiplex networks. *Science*. 328:876–878.

Owen AM, Coleman MR, Boly M, Davis MH, Laureys S, Pickard JD. 2006. Detecting awareness in the vegetative state. *Science*. 313:1402.

Peduto VA, Concas A, Santoro G, Biggio G, Gessa GL. 1991. Biochemical and electrophysiologic evidence that propofol enhances GABAergic transmission in the rat brain. *Anesthesiology*. 75:1000–1009.

Peltier SJ, Kerssens C, Hamann SB, Sebel PS, Byas-Smith M, Hu X. 2005. Functional connectivity changes with concentration of sevoflurane anesthesia. *Neuroreport*. 16:285–288.

Shmuel A, Leopold DA. 2008. Neuronal correlates of spontaneous fluctuations in fMRI signals in monkey visual cortex: implications for functional connectivity at rest. *Hum Brain Mapp*. 29:751–761.

Sitt JD, King J-R, El Karoui I, Rohaut B, Faugeras F, Gramfort A, Cohen L, Sigman M, Dehaene S, Naccache L. 2014. Large scale screening of neural signatures of consciousness in patients in a vegetative or minimally conscious state. *Brain*. 137:2258–2270.

Sizemore AE, Bassett DS. 2018. Dynamic graph metrics: tutorial, toolbox, and tale. *Neuroimage*. 180:417–427.

Spoormaker VI, Gleiser PM, Czisch M. 2012. Frontoparietal connectivity and hierarchical structure of the Brain's functional network during sleep. *Front Neurol*. 3:1–10.

Sporns O, Betzel RF. 2016. Modular brain networks. *Annu Rev Psychol*. 67:613–640.

Tagliazucchi E, von Wegner F, Morzelewski A, Brodbeck V, Borisov S, Jahnke K, Laufs H. 2013. Large-scale brain functional modularity is reflected in slow electroencephalographic rhythms across the human non-rapid eye movement sleep cycle. *Neuroimage*. 70:327–339.

Telesford QK, Ashourvan A, Wymbs NF, Grafton ST, Vettel JM, Bassett DS. 2017. Cohesive network reconfiguration accompanies extended training. *Hum Brain Mapp*. 38:4744–4759.

Tononi G. 2004. An information integration theory of consciousness. *BMC Neurosci*. 5:42.

Tononi G, Boly M, Massimini M, Koch C. 2016. Integrated information theory: from consciousness to its physical substrate. *Nat Rev Neurosci*. 17:450–461.

Uhrig L, Sitt JD, Jacob A, Tasserie J, Barttfeld P, Dupont M, Dehaene S, Jarraya B. 2018. Resting-state dynamics as a cortical signature of anesthesia in monkeys. *Anesthesiology*. 129:942–958.

Van Essen DC. 2004. Surface-based approaches to spatial localization and registration in primate cerebral cortex. *Neuroimage*. 23:S97–S107.

Vincent JL, Patel GH, Fox MD, Snyder AZ, Baker JT, Van Essen DC, Zempel JM, Snyder LH, Corbetta M, Raichle ME. 2007. Intrinsic functional architecture in the anaesthetized monkey brain. *Nature*. 447:83–86.

Wagner GP. 2005. Robustness and Evolvability in Living Systems. Princeton, NJ: Princeton University Press.

Wu J, Harata N, Akaike N. 1996. Potentiation by sevoflurane of the gamma-aminobutyric acid-induced chloride current in acutely dissociated CA1 pyramidal neurones from rat hippocampus. *Br J Pharmacol*. 119:1013–1021.